ChemPubSoc Europe

DOI: 10.1002/cphc.201900703

CHEMPHYSCHEM Articles

Addressing Charge-Transfer and Locally-Excited States in a Twisted Biphenyl Push-Pull Chromophore

Elisa Campioli,[a] Somananda Sanyal,[a] Agnese Marcelli,[b] Mariangela Di Donato,[b] Mireille Blanchard-Desce,[c] Olivier Mongin,[d] Anna Painelli,[a] and Francesca Terenziani*[a]

We present the synthesis and spectroscopic characterization of a twisted push–pull biphenyl molecule undergoing photo-induced electron transfer. Steady-state and transient absorption spectra suggest, in this rigid molecular structure, a subtle interplay between locally-excited and charge-transfer states, whose equilibrium and dynamics is only driven by solvation. A theoretical model is presented for the solvation dynamics and, with the support of quantum chemical calculations, we demonstrate the existence of two sets of states, having either local or charge-transfer character, that only "communicate" thanks to solvation, which is the sole driving force for the charge-separation process.

1. Introduction

Electron transfer is a widespread and widely exploited process in many different fields, from life-sustaining reactions and photosynthesis,[1] to molecular electronics,[2,3] light-emitting devices[4] and solar cells.[5,6] The understanding of charge-transfer processes has enormously deepened in the last years thanks to new experimental techniques (among which time-resolved spectroscopy) and sophisticated computational tools.[7,8] Electron transfer is affected and controlled by many variables, including temperature, donor-acceptor distance, coupling to nuclear degrees of freedom and solvation.[7–10] In this context, systems where the electron-donor and the electron-acceptor group are covalently linked through a rigid spacer are particularly useful molecular models,[11] where the process is typically referred to as an intramolecular electron (or charge) transfer event.

Substituted and/or rigidified dialkylaminobenzonitriles,[10,12–15] bianthryl molecules,[16–21] substituted biphenyl derivatives[22–26] have been extensively investigated as model systems to unravel the vibrational and solvation effects in photoinduced intramolecular electron transfer. All these molecules are characterized by at least one conformational degree of freedom strongly coupled to the charge-transfer process: the rotation of the amino group in aminobenzonitriles, the angle between the planes of the two anthryl or phenyl rings in bianthryl and biphenyl derivatives. Different substitutions and derivatizations have been performed on those systems,[12–14,17,22–27] in order to facilitate or inhibit the motion along the coupled nuclear coordinate and investigate its effects on the charge-transfer process. Controlling the coupling of the charge-transfer process with nuclear degrees of freedom helps to single out the effects of solvation. The interaction with the solvent plays a strong role in electron-transfer processes since charge-transfer states are characterized by large permanent dipole moments and hence strongly interact with polar solvents. Optical spectra of model systems for electron transfer are often characterized by a subtle interplay between locally-excited (LE) and charge-transfer (CT) states, strongly affected by the solvent. Many of these systems display dual fluorescence in polar solvents[12–15,28,29] and show transient optical behavior strongly dependent on the solvent itself.[17–19,23,26]

In this paper, we investigate a push-pull substituted biphenyl compound (hereafter TBP) where the electron-donor and the electron-acceptor groups are connected to the biphenyl central core via extended π-conjugated bridges favoring long-distance electron transfer. Various "push-push", "pull-pull" and "push-pull" systems have been reported in the literature based on functionalized biphenyl cores,[26,27] with applications in two-photon absorption,[30–32] sensing,[33] light-emitting devices,[34] solar energy conversion.[29,34,35] The extent of π overlap in the two benzene rings affects the extent of electronic delocalization over the entire π system. This varies with the torsional angle between the planes of the two phenyl rings. Specifically, a large conjugation is expected for a biphenyl system with coplanar phenyl rings. On the other hand, delocalization is disrupted in compounds where the two rings are mutually orthogonal. Thermal motion and the presence of substituents in different positions affect the torsional angle, with strong effects on the molecular photophysics.[26,27,29]

In the investigated compound, the 2,2′ and 6,6′ positions of the biphenyl are substituted by methyl groups, whose steric hindrance imposes a large twist of the two phenyl rings, resulting in a very poor conjugation between the two halves of

[a] Dr. E. Campioli, Dr. S. Sanyal, Prof. Dr. A. Painelli, Prof. Dr. F. Terenziani
Dipartimento di Scienze Chimiche, della Vita e della Sostenibilità Ambientale, Università di Parma
Parco Area delle Scienze 17/A, 43124 Parma, Italy
E-mail: francesca.terenziani@unipr.it
[b] Dr. A. Marcelli, Dr. M. Di Donato
LENS, via N. Carrara 11, 50019 Sesto Fiorentino (FI), Italy
[c] Dr. M. Blanchard-Desce
Univ. Bordeaux
Institut des Sciences Moléculaires (CNRS UMR 5255)
33405 Talence, France
[d] Dr. O. Mongin
Univ Rennes
CNRS, ISCR (Institut des Sciences Chimiques de Rennes)
UMR 6226, 35000 Rennes, France

Supporting information for this article is available on the WWW under https://doi.org/10.1002/cphc.201900703

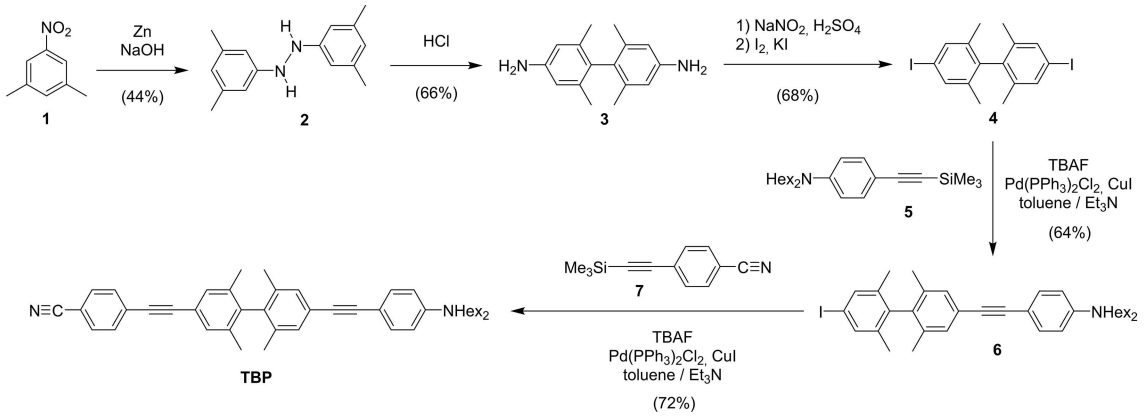

Scheme 1. Scheme of the synthesis of **TBP.**

the molecule and hindering the rotation around the central C–C bond. Accordingly, conformational motion can be disregarded, leaving solvation as the only coordinate coupled to the electron transfer process. Upon photoexcitation, a long-distance and long-lived charge-transfer state is observed, whose photophysics is governed by polar solvation. In particular, we analyze the interplay between the LE and CT states in solution by means of steady-state and time-resolved optical spectroscopy, as well as by making resort to essential-state models and quantum chemical calculations. We do not limit the investigation to the first LE and CT states, but recognize and identify two distinct manifolds of LE and CT states that are not optically coupled and can interconvert only thanks to solvation after photoexcitation.

2. Results and Discussion

TBP was synthesized in a five-step sequence (Scheme 1) from commercially available 3,5-dimethylnitrobenzene (**1**). Reduction of **1** in the presence of zinc powder and sodium hydroxide led to hydrazine **2**,[36,37] the Zinin rearrangement of which, performed in refluxing HCl (10%), afforded 2,2′,6,6′-tetramethylbenzidine (**3**).[36,37] Diazotization of both amino groups of **3** and treatment of the resulting diazonium salt with potassium iodide and iodine gave the diiodo derivative **4**.[37,38] Finally, **TBP** was obtained from the latter compound by two successive Sonogashira couplings with alkynes **5**[39] and **7**[40] (deprotected in situ with TBAF).

2.1. Steady-State Spectroscopy

TBP is a push-pull D-π-A molecule where a dialkylamino donor group (D) and a cyano acceptor group (A) are connected to a biphenyl moiety through extended π bridges (Scheme 1). The 2,2′ and 6,6′ positions of the biphenyl bear methyl groups, whose steric hindrance forces the two phenyl rings to be almost perpendicular to one another in the ground state, as suggested by the crystallographic structure of similar compounds,[27] and confirmed by quantum-chemical calculations (see computational part). The twisted biphenyl structure forces very small conjugation between the donor and the acceptor sides of the molecule, so that the CT transition is expected to have very low intensity.

The absorption and emission spectra of TBP were measured in solvents of different polarity, namely cyclohexane, toluene, diethyl ether, tetrahydrofuran (THF), triacetin, dichloromethane (DCM), dimethyl sulfoxide (DMSO), as well as in the solid and nanoaggregate state. Spectra are reported in Figure 1, and main spectral properties are summarized in Table 1.

The absorption spectrum is characterized by a band with a pronounced vibronic structure, with a maximum centered at ~325 nm. When increasing the solvent polarity, no appreciable shift of the band is observed, while a broadening occurs when going from the nonpolar solvent cyclohexane to more polar solvents. The oscillator strength associated to the absorption band amounts to ~4.5, corresponding to a transition dipole moment of ~10 D. Such an intense band cannot be assigned to the charge transfer transition from the donor to the acceptor moiety since the twisted structure suggests very low intensities for CT bands. We then assign the absorption band to a transition toward a LE state. LE states in TBP can be related to excitations involving separately the two halves of the molecule, each half corresponding to a substituted diphenylacetylene (also called tolane).

The solvent dependence of the fluorescence spectrum is fairly complex and very interesting. In cyclohexane a strong emission is detected (quantum yield of 65%, lifetime 0.7 ns), partly overlapping with the absorption band. For increasing solvent polarity, the emission band progressively shifts to the red and loses intensity, the quantum yield reducing to less than 1% in DCM (in this solvent the radiative decay rate is two orders of magnitude smaller than the non-radiative decay rate, see Table 1). The fluorescence signal is vanishingly small in more polar solvents (acetonitrile and DMSO). In medium/high polarity solvents (diethyl ether, THF, triacetin and DCM) a dual emission is observed, with the main band located at long wavelengths in a position depending on the solvent polarity, and a second band located in the same position as the emission band recorded in cyclohexane.

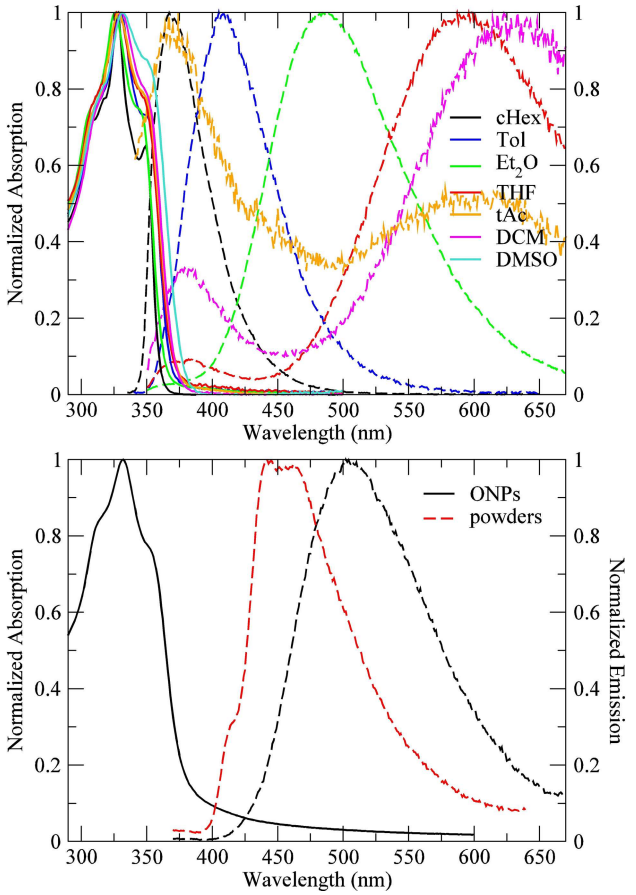

Figure 1. Top panel: Absorption and emission spectra of TBP in solvents of different polarity (cyclohexane = cHex; toluene = Tol; diethyl ether = Et_2O; tetrahydrofuran = THF; triacetin = tAc; dichloromethane = DCM; dimethyl sulfoxide = DMSO). Bottom panel: Absorption and emission spectra of TBP as ONPs in water suspension (black lines) and in the solid state (only emission, red line).

The emission in cyclohexane is easily explained as stemming from the same LE state responsible for the lowest-energy absorption band. The residual emission observed in higher-polarity solvents in the same spectral position is quite naturally ascribed to the same LE state (the associated lifetime, similar to the one measured in cyclohexane, confirms this hypothesis). Since LE states are localized on each single half of the molecule, emission from the lowest-energy LE state of TBP is related to the emission of a substituted tolane. As discussed in the literature,[41–43] tolane emission typically stems from a relaxed trans-bent geometry. The strongly solvatochromic emission observed at longer wavelengths has a clear CT origin. Since fluorescence emission typically stems from the lowest-energy excited state, this behavior suggests that the lowest-energy excited state has a LE nature in nonpolar solvents, and a CT character in polar solvents, in agreement with a stabilization of the CT state in polar solvents. The residual emission observed from the LE state in polar solvents is explained in terms of a very small population residing on the LE state and is justified by the very different radiative emission rates associated to the LE and CT states (Table 1, compare k_r in cyclohexane with values in polar solvents). Moreover, the intensity of the residual emission band from the LE state depends on the solvent and can be related to the typical solvation time: in triacetin, a polar solvent characterized by a very slow relaxation time, the residual emission from the LE state is even more intense than the CT emission.

The transition dipole moment associated with fluorescence can be estimated from the radiative decay rate according to the Fermi's golden rule for spontaneous emission:[44] we obtain values of ~12 D in cyclohexane, ~5 D in toluene, decreasing down to ~1 D in DCM. These values are in agreement with the interpretation of the emission stemming from a strongly allowed LE state in the nonpolar solvent (in fact the transition dipole moments associated to absorption and emission are very similar in cyclohexane), and related to an almost forbidden CT transition in polar solvents. Toluene seems to be an intermediate case, where the excited-state population could be distributed on both types of states, suggesting that the solvent-equilibrated LE and CT states are almost degenerate in that solvent.

Table 1. Main spectral properties of TBP in solvents of different polarity and in the solid and nanoaggregate state.

	λ_{abs} [a] [nm]	ε_{max} [b] [$M^{-1}cm^{-1}$]	λ_{em} [c] [nm]	τ [d] [ns]	Φ [e]	k_r [f] [10^8 s^{-1}]	k_{nr} [g] [10^8 s^{-1}]
Cyclohexane	327	72600	367	0.70	0.650	9.28	5.00
Toluene	329	–	409	4.08	0.470	1.15	1.30
Diethyl ether	326	–	484	11.7	0.150	0.13	0.72
THF	328	64100	377	-	0.024	0.04	1.63
			592	6.00			
Triacetin	328	–	370	< 0.5 [h]	0.031	–	–
			600	2.06 (88%); 6.90 (12%)			
DCM	331	–	377	–	0.005	0.01	3.68
			625	2.06 (95%); 9.39 (5%)			
DMSO	331	–	–	–	–	–	–
Powders	–	–	443	4.64 (9%); 25.5 (23%); 0.8 (68%)	–	–	–
ONPs	332	49200	504	3.64 (2%); 23.6 (27%); 66.5 (71%)	0.06	–	–

[a] Wavelength of maximum absorption (±1 nm). [b] Molar extinction coefficient at the wavelength of maximum absorption (±5%). [c] Wavelengths of maximum emission (±2 nm). [d] Fluorescence lifetime(s) (and corresponding relative amplitudes) extracted from the fit of the fluorescence decay measured at the wavelength reported in the same line of column c (excitation wavelength 340 nm). [e] Fluorescence quantum yield (±10%). [f] Radiative decay rate obtained from quantum yield and (average) lifetime. [g] Non-radiative decay rate. [h] Shorter than the instrumental response.

According to our interpretation, in the nonpolar solvent absorption and emission involve the same state with a strong LE character, while in polar solvents the vertical excitation still populates a state with strong LE nature, but emission stems from the relaxed excited state, which has a dominant CT character.

The LE/CT excited-state scenario extracted from steady-state and lifetime data is summarized in Scheme 2, where the role of polar solvation in driving the relaxation from the LE to the CT state is underlined, and the timescales of the competitive decay processes are reported.

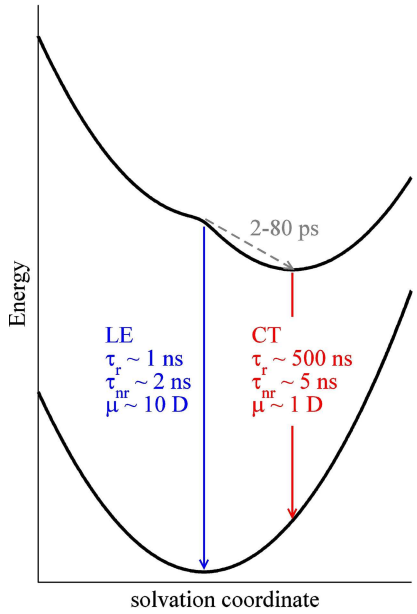

Scheme 2. Energy diagram of the lowest-energy electronic singlet states and possible radiative and non-radiative transitions of **TBP** in polar solvents (after fast solvent relaxation). In blue: decay from the LE state to the ground state, with associated radiative and non-radiative lifetimes and transition dipole moment. In red: the decay from the CT state to the ground state, with associated radiative and non-radiative lifetimes and transition dipole moment. In grey: the non-radiative, spontaneous decay from the LE to the CT state, driven by the slow component of solvent relaxation, with a timescale depending on the specific solvent.

An interesting characteristic of the CT state is the associated lifetime, amounting to ~10 ns in polar solvents: such a long-lived charge-separated state could be of interest, for example, in solar energy conversion applications. In order to test if this property is preserved in the solid state, we characterized the spectroscopic properties of TBP powders. The powders are significantly fluorescent (quantum yield not estimated), with a spectrum (Figure 1, bottom panel) that resembles the emission spectrum in a low-polarity solvent (something in between toluene and diethyl ether). Much as in solution, we recognize a dual fluorescence behavior: a weak band at shorter wavelength (ascribed to a residual emission from the LE state) and a more intense band at ~440 nm (ascribed to the emission from the CT state). The 3-exponential decay of the fluorescence is characterized by a > 20 ns component with a ~30% weight, confirming the long-living character of the CT state in the solid state.

Organic nanoparticles (ONPs) in water suspension were also prepared, to evaluate the effect of nanoaggregation. Absorption and fluorescence spectra are reported in Figure 1, bottom panel. The absorption spectrum is very similar to the absorption spectra measured in solution and the emission band basically recovers the fluorescence measured in diethyl ether solution (with similar quantum yield, 6% vs 15%), suggesting that the environment experienced by the molecules in the ONPs has a polarity very close to that solvent. The main component of the 3-exponential decay of the fluorescence intensity is the longest one, amounting to ~66 ns, confirming again the long-living nature of the CT state. In none of the aggregated states we observed excitonic effects: the main effect of intermolecular interactions in the nanoaggregates and in the microcrystals is that of a dielectric continuum.

2.2. Theoretical Modeling of Steady-State Spectra

To model a D-π-A push-pull molecule with a CT/LE interplay through an essential-state description, three basis (diabatic) states have to be introduced: the neutral form $|D\text{-}\pi\text{-}A>$, the charge-separated form $|D^+\text{-}\pi\text{-}A^->$ (a pure CT state), and a locally excited basis state that we denote with $|D\text{-}\pi^*\text{-}A>$ (a pure LE state). The electronic Hamiltonian is defined by the energies associated with these three basis states, respectively 0, 2η and 2ζ, and by the mixing matrix elements: $<D\text{-}\pi\text{-}A|H|D^+\text{-}\pi\text{-}A^->=-\tau$, and $<D\text{-}\pi^*\text{-}A|H|D^+\text{-}\pi\text{-}A^->=-\beta$.[45] We define the dipole moment operator in terms of μ_0, the dipole moment of the zwitterionic $|D^+\text{-}\pi\text{-}A^->$ state, which is very large if compared with $<D\text{-}\pi\text{-}A|\mu|D\text{-}\pi\text{-}A>$ and $<D^+\text{-}\pi\text{-}A^-|\mu|D\text{-}\pi\text{-}A>$, so that the last two can be approximated to 0. To account for the intensity of the LE transition, we introduce an additional matrix element of the dipole-moment operator: $<D\text{-}\pi\text{-}A|\mu|D\text{-}\pi^*\text{-}A>=\mu_{e^*}$.[45]

Polar solvation is described introducing the electric field F generated by the orientation of the polar solvent molecules around the solute. F stabilizes the zwitterionic $|D^+\text{-}\pi\text{-}A^->$ basis state, so that its energy becomes $2\eta\text{-}\mu_0 F$. If the solute is described as a continuum elastic medium, an additional term, $(\mu_0 F)^2/(4\varepsilon_{or})$, enters the Hamiltonian to account for the elastic energy needed to create the field, where ε_{or} measures the solvent reorganization energy. F describes a slow motion and is dealt with in the adiabatic approximation.[45] The diagonalization of the F-dependent electronic problem then leads to F-dependent eigenvalues, i.e. the adiabatic potential energy surfaces (PES) as reported in Figure 2. As a reference, the diabatic states are also shown as colored lines. In the specific case, the twisted geometry implies a small mixing, and the ground state strongly resembles the neutral $|D\text{-}\pi\text{-}A>$ form. The two excited states result from the mixing of the pure CT and pure LE basis states, but the mixing is significant only in the region where the LE and CT basis states are almost degenerate (see the zoom in Figure 2). In particular, focusing on the lowest-energy excited state (the one relevant to fluorescence), we can

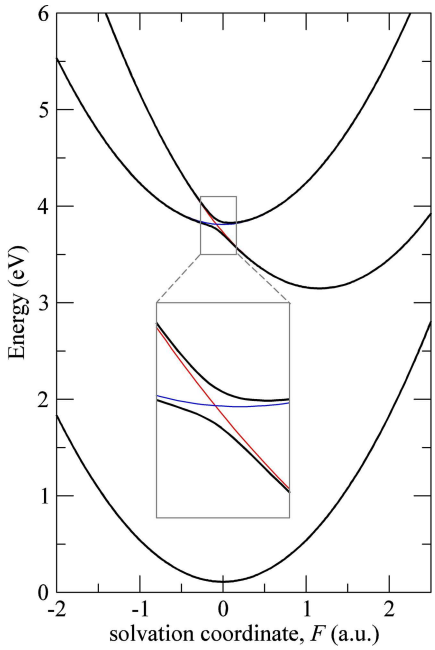

Figure 2. Potential energy surfaces relevant to the diabatic basis states (colored lines) and to the adiabatic eigenstates (black full lines) as a function of the solvation coordinate. The diabatic curve relevant to the $|$D-π-A$>$ state is superimposed to the ground-state curve. The inset shows a magnification of the region where the diabatic LE (blue line) and CT (red line) states cross.

recognize an almost pure LE character for negative values of the solvation coordinate, and an almost pure CT character for positive values of the solvation coordinate. In other words, in polar solvents the vertical excitation leads to a state having a mixed LE/CT nature, with the transition having mainly a LE character (because of the very small transition dipole moment associated to the CT transition). After photoexcitation we expect that the system relaxes along the solvation coordinate, reaching the minimum of the PES, characterized by a strong (almost pure) CT nature.

To complete the model, we introduce an effective harmonic vibrational coordinate, $Q*$, with frequency $\omega*$. The diabatic $|$D-π*-A$>$ state has displaced minimum with respect to $|$D-π-A$>$ along $Q*$, so that the energy gaps acquire a linear dependence on $Q*$: $2\xi - \omega*\sqrt{2\varepsilon*}Q*$, where $\varepsilon*$ is the vibrational relaxation energy.[45] We do not insert any vibrational coordinate coupling the pure CT state with the ground state because, in this specific molecule, the twisted structure hinders any significant contribution of nuclear motion to the charge-transfer process.

The adiabatic approximation safely applies to the solvation coordinate, but it must be carefully evaluated when dealing with vibrational motion. In fact, the adiabatic approximation is doomed to fail whenever the energy difference between the electronic states becomes comparable to the vibrational quanta, as it is the case for the LE/CT three-level model. We therefore rely on the direct diagonalization of the nonadiabatic Hamiltonian matrix.[45] Briefly, for fixed F values, the (F-dependent) Hamiltonian matrix is written on the basis obtained as the direct product of the electronic diabatic states and the eigenstates of the harmonic oscillators associated with each vibrational coordinate. The nominally infinite basis associated with the oscillator is truncated to the M lowest states. The Hamiltonian matrix is then diagonalized to get numerically exact vibronic eigenstates, provided M is large enough to get convergence ($M=10$ is used here). Transition and permanent dipole moments are calculated from the eigenvectors. Steady-state optical spectra are finally obtained as sum of spectra obtained for different F-values, weighting each spectrum for the relevant Boltzmann distribution. Specifically, the ground-state Boltzmann distribution applies to absorption spectra while, for fluorescence spectra, the Boltzmann distribution must be calculated based on the energy of the emitting state.[46]

The nonadiabatic approach is conceptually simple and applies smoothly even to difficult cases where large anharmonicities are present and/or several electronic states have similar energies. Its main drawback is that it hinders the classification of excited states as "vibrational" or "electronic": all nonadiabatic eigenstates are indeed "vibronic". This is not an issue in the calculation of absorption spectra but, to calculate fluorescence spectra, the emissive state must be identified as the lowest excited state with electronic character. This is possible through a detailed analysis of the eigenvectors and/or a comparison of transition dipole moments from the ground state (electronic transitions are typically characterized by much larger transition dipole moments than vibrational ones) or permanent dipole moments (CT states are characterized by large permanent dipole moments).[45,47]

In the essential-state approach, the model parameters are fixed as to best reproduce the available experimental data, namely absorption and emission spectra. Best results for TBP are obtained with the model parameters reported in Table 2. Calculated absorption and emission spectra (Figure 3) compare well with the experimental data: in particular, the solvent polarity mainly affects emission spectra, with a strong positive solvatochromic effect, while absorption spectra are barely affected. The intensity of emission, even if the spectra have been normalized in Figure 3, is also well reproduced, decreasing of a factor of ~200 from the less polar to the most polar solvent.

Table 2. Molecular model parameters entering the calculation of the optical spectra of TBP, as discussed in the text. $\Gamma=0.06$ eV is the effective intrinsic width assigned to each transition.

η [eV]	τ [eV]	ζ [eV]	β [eV]	μ_0 [D]	μ_* [D]	ω_* [eV]	ε_* [eV]
1.81	0.02	1.85	0.05	20	8	0.12	0.16

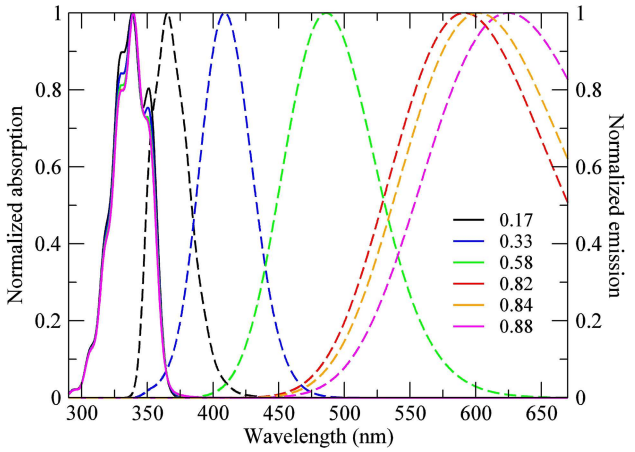

Figure 3. Calculated absorption and emission spectra using the model parameters reported in Table 2. The spectra of different color simulate different solvents (ε_{or} values in the legend).

2.3. Transient Spectroscopy

To obtain more information on the nature of the excited states and on the evolution from a state having LE character to a state having CT character, we performed transient absorption measurements in solvents of different polarity and different relaxation times (Figure 4). The pump pulse was centered at 330 nm, while the broadband probe pulse covered the 400–650 nm spectral region.

The positive band dominating the differential absorption spectra is due to excited-state absorption (ESA) from the state(s) populated by the pump pulse, toward higher-energy excited state(s). In cyclohexane (Figure 4a), this band does not show any appreciable temporal evolution, apart from a progressive decrease in intensity due to the depopulation of the excited state itself, on a timescale somewhat shorter than 1 ns, in agreement with the measured fluorescence lifetime (Table 1).

Much more interesting is the dynamics of pump-probe spectra measured in polar solvents. In all polar solvents (diethyl ether, triacetin, DMSO), two ESA bands are observed in the transient spectra, located at about 500 and 450 nm. The relative intensity of the two bands changes with the time delay: for short pump-probe delays, the long-wavelength feature dominates, while at longer time delays the short-wavelength band appears, progressively acquiring intensity at the expense of the long-wavelength band. The kinetics of this evolution is clearly governed by solvation. In fact, while the evolution of the spectral shape is qualitatively similar in all polar solvents, the associated times are clearly solvent-dependent, being faster in diethyl ether than in DMSO, and much slower in triacetin, as shown by the kinetic traces in Figure 5, relevant to the decay of the long-wavelength band.

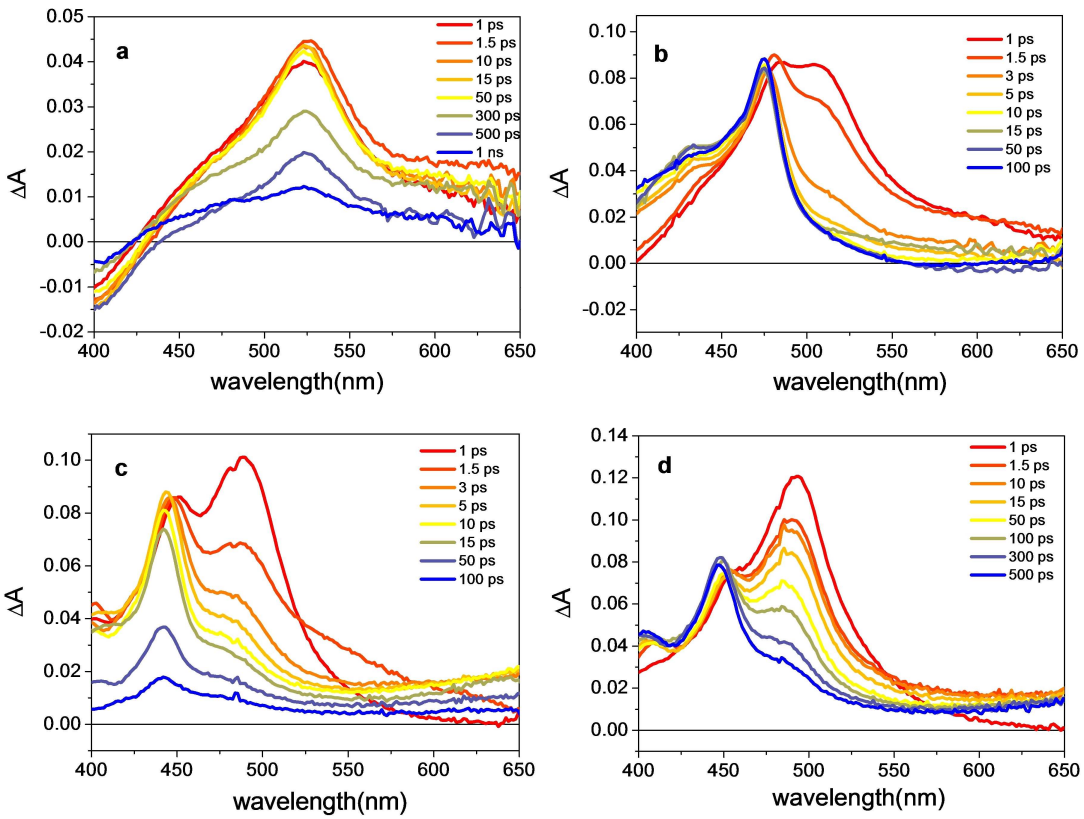

Figure 4. Transient pump-probe spectra measured in a) cyclohexane, b) diethyl ether, c) DMSO, and d) triacetin.

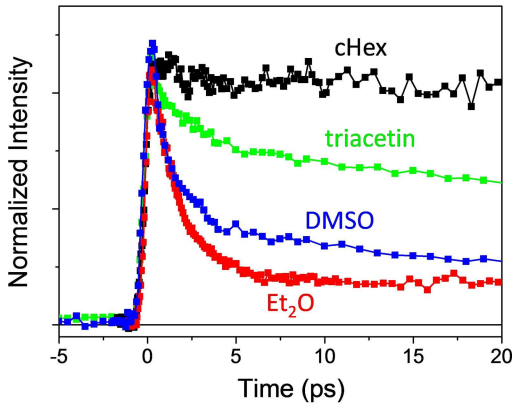

Figure 5. Decay of the long-wavelength band in different solvents: cyclohexane (cHex, black), diethyl ether (Et_2O, red), DMSO (blue), triacetin (green).

The two features observed in the transient absorption spectra can be ascribed to ESA processes occurring from the LE and CT states. Specifically, the long-wavelength feature, losing intensity with time delay, is ascribed to ESA from the LE state, which is directly populated by the pump pulse, and progressively depopulates towards the CT state on the typical solvation timescale. The short-wavelength signal corresponds to ESA from the CT state, which is stabilized by polar solvation. In other terms, after the excitation the population flows on a potential energy surface (along the solvation coordinate) having a strong LE character at zero time and a strong CT character when solvation is accomplished. In transient spectra the feature related to ESA from the LE state gradually disappears in favour of the ESA feature from the CT state, with a nice temporary isosbestic point (for times significantly shorter than the excited-state lifetime) confirming an equilibrium between two states.

To get quantitative information on the kinetics of excited state relaxation involving the conversion from the LE to the CT state, the transient absorption data recorded in different solvents were analyzed using singular value decomposition[48,49] and global analysis,[50] which consists in simultaneously fitting the kinetics at all the recorded wavelengths with a combination of exponential functions. Global analysis was performed by imposing a simple sequential kinetic decay scheme. Except for DMSO, where four kinetic constants were used, three kinetic constants were sufficient for a satisfactory fit of the data. Besides kinetic constants, global analysis also retrieves the associated spectral components, called Evolution Associated Difference Spectra (EADS), which are shown in Figure 6 for all the investigated solvents.

Inspection of the EADS highlights that the kinetics of the interconversion between the LE and CT states depends on the solvent properties. In cyclohexane (Figure 6a) the spectral

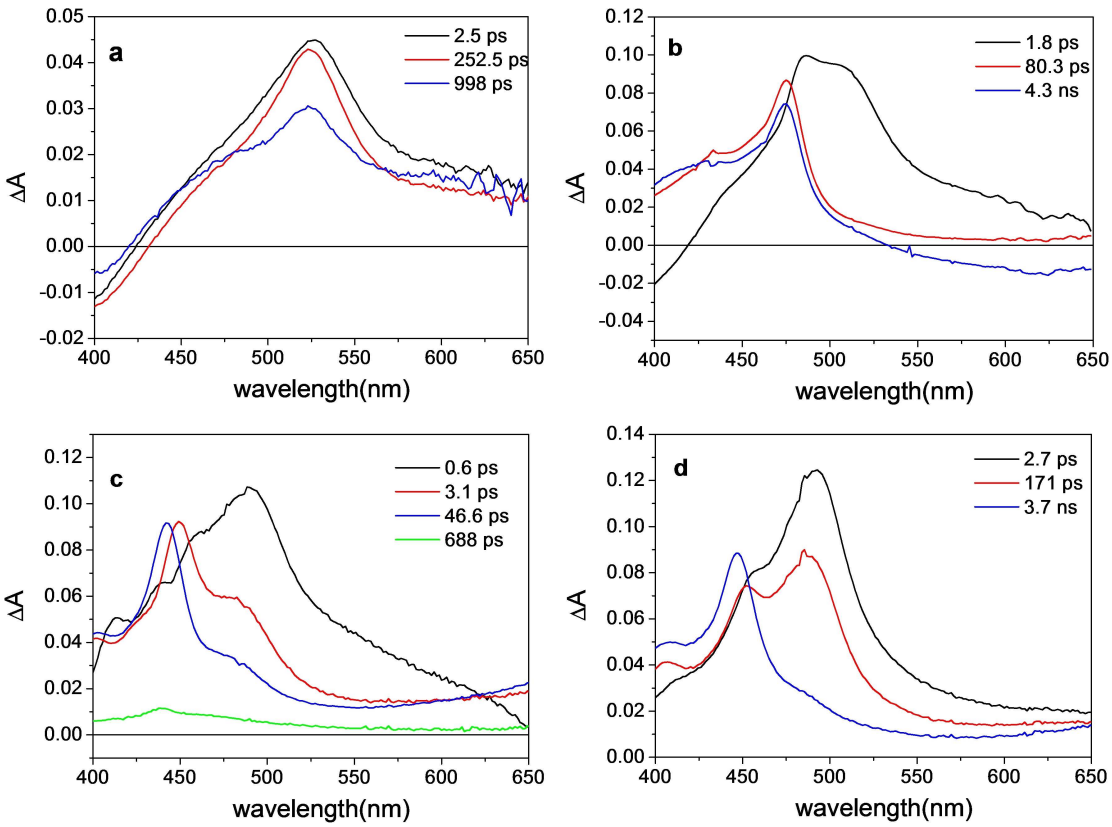

Figure 6. EADS obtained from global analysis of transient absorption data of TBP recorded in: a) cyclohexane, b) diethyl ether, c) DMSO, and d) triacetin. The lifetimes associated to each spectral component are reported on each panel.

evolution is very limited, suggesting that no significant dynamics occurs other than the slow relaxation of the LE state to the ground state (on a timescale of about 1 ns, in agreement with the measured fluorescence lifetime). In fact, cyclohexane is a non-polar solvent, so that no significant solvation is expected. In all the other solvents, a conversion from the LE to the CT state is evident, showing a kinetic behavior highly dependent on the solvent. In diethyl ether (Figure 6b), the positive band in the first EADS (broad feature peaking at about 520 nm, black line) can be interpreted as the ESA from the LE state. In 1.8 ps this spectral component evolves towards the second one (red line), where the positive band peaks at 475 nm and is assigned to the ESA from the CT state. The intensity of this band slightly decreases in about 80 ps and then finally recovers on a long 4 ns timescale. When going to the more polar solvent DMSO (Figure 6c), the relaxation from the LE to the CT state appears to occur bi-exponentially on a 0.6 ps and 3.1 ps timescales (evolution from black to red and red to blue EADS). The lifetime of the excited state in this solvent is reduced compared to diethyl ether: most of the transient signal in fact recovers on a 46 ps timescale, and only a small residual signal decays on the ns timescale, in agreement with the poor fluorescence quantum yield in this solvent. Finally, in triacetin (Figure 6d) the conversion between the LE and CT states occurs on a significantly longer timescale and is complete in about 170 ps. The excited-state lifetime is quite long in this solvent, being on the order of 3.7 ns. Our analysis clearly shows that the evolution of the excited-state population from the LE to the CT state in medium/high polarity solvents is dictated by the solvent properties. The associated times in fact compare well with the typical solvation times reported in the literature for the three solvents: 1.7 ps for diethyl ether,[51] 3.1 ps for DMSO,[52] 80 ps for triacetin.[53]

A puzzling feature of transient spectra is that neither the band assigned to excited-state absorption from LE state, nor the band assigned to excited-state absorption from the CT state show any significant solvatochromism nor any significant shift with the time delay (the shifts are on the order of 1000 cm^{-1}, i.e. not larger than a typical vibrational frequency). This is particularly surprising for the feature ascribed to the CT state, since our data demonstrate that the energy of the lowest-energy CT state is very sensitive to solvation (see e.g. the large emission solvatochromism). This result can be rationalized assuming that the state reached upon ESA from the low-lying CT state has a very similar solvatochromic behavior, i.e. it has a similar CT nature as the low-lying CT state, so that their energy difference stays roughly constant. Analogously, the excited-state reached upon absorption from the LE state should have a LE character too.

2.4. Modeling Solvation Dynamics

In the pump-probe experiment, a UV or visible pulse creates an out-of-equilibrium population in the resonant excited state. A delayed broad-band UV-vis pulse then addresses the spectral properties of the system while the population evolves towards

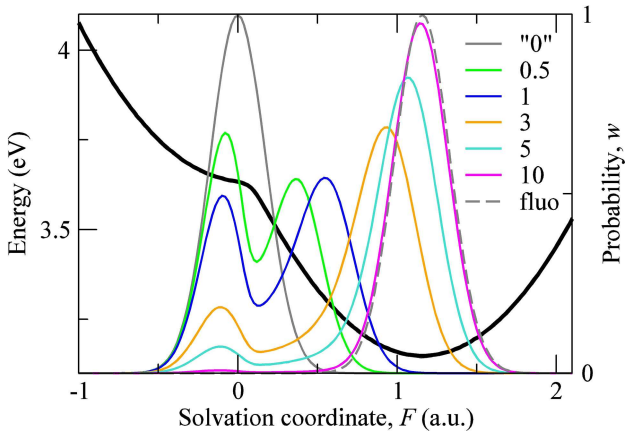

Figure 7. The energy of the emissive excited state (thick black line) as a function of the solvation coordinate, calculated for TBP in diethyl ether (model parameters in Table 2; $\varepsilon_{or} = 0.58$ eV, $\tau_s = 1.7$ ps). The probability distribution of the solvation coordinate is reported for different pump-probe delay times (lines of different colors, each labeled by the corresponding delay time, in ps, measured with respect to the effective zero time of solvation). The probability distributions of the solvation coordinate relevant to the effective zero-time of solvation (labeled "0") and to the relaxed excited state (labeled fluo) are reported as grey lines.

the excited-state equilibrium and finally relaxes back to the ground state. To mimic the experiment, we describe the dynamics of an excited system, obtained populating, via a vertical transition, the state responsible for steady-state emission (whose energy, as a function of the reaction field, is reported in Figure 7 as a black thick line).[47,54] This defines an effective zero time where vibrational cooling already occurred, while the solvent distribution is still frozen in the same configuration as in the ground state.[54] We are thus assuming that, after photoexcitation, vibrational coordinates relax on a faster timescale with respect to solvation, so that it is possible to separate the vibrational and solvation motions, assuming that solvation dynamics starts after vibrational cooling.[55] The zero-time distribution of the reaction-field coordinate (the solvation coordinate) is shown in Figure 7 as a grey full line (labeled "0"), while the thermally-equilibrated distribution relevant to the excited state is reported as a grey dashed line (labeled fluo). This relaxed distribution is calculated as the Boltzmann distribution relevant to the emissive state.

The evolution of the probability distribution from the effective zero time to the fully relaxed limit is calculated using the Smoluchowski diffusion equation [Eq. (1)]:[56]

$$\frac{\partial w(F,t)}{\partial t} = \frac{1}{\tau_s}\left[w(F,t)\frac{\partial^2 V(F)}{\partial F^2} + \frac{\partial V(F)}{\partial F}\frac{\partial w(F,t)}{\partial F} + kT\frac{\partial^2 w(F,t)}{\partial F^2}\right] \quad (1)$$

where w is the F- and t-dependent probability distribution, $V(F)$ is the PES governing the evolution, τ_s is the average solvation time (typical of each solvent), k is the Boltzmann constant and T the temperature (set to 298 K). Consistently with the separation between nuclear and solvation dynamics, vibrational and electronic degrees of freedom are assumed to be always in

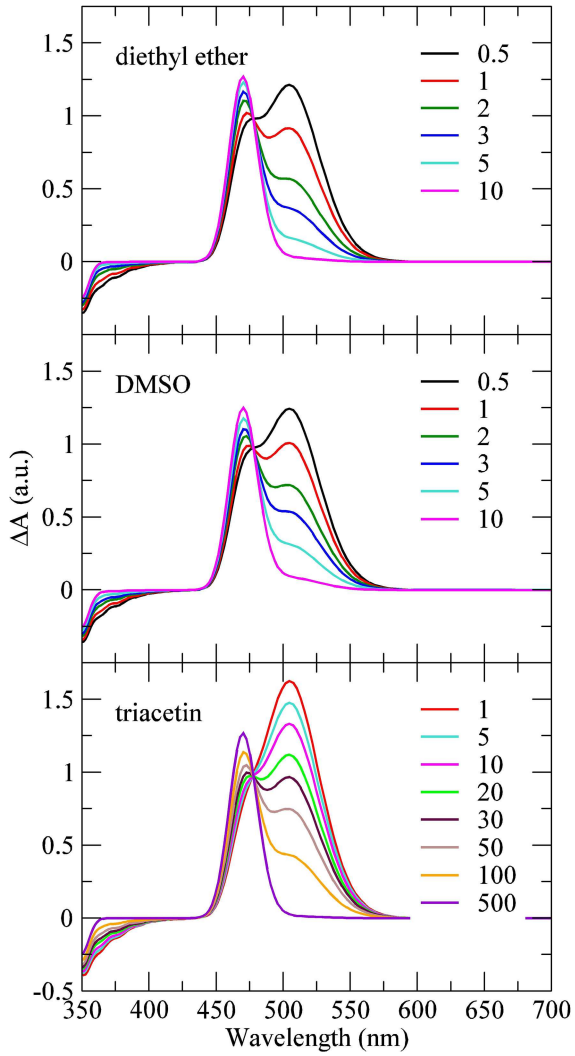

Figure 8. Calculated pump-probe (differential absorption) spectra for TBP in different solvents (model parameters in Table 2; $\varepsilon_{or} = 0.58$, 0.88, 0.84 eV and $\tau_s = 1.7$, 3.1, 80 ps for diethyl ether, dimethyl sulfoxide and triacetin, respectively) for variable delay time (expressed in ps, see legends).

equilibrium with the instantaneous configuration of the solvent.[54]

Results about the evolution of the *F*-distribution with time, reported in Figure 7, are calculated setting $\tau_s = 1.7$ ps, as relevant to diethyl ether.[51] Calculated distributions are shown as colored lines for selected delay times (specified by the labels). The distribution evolves along a PES characterized by a double-minimum shape with no barrier in between the two minima. The zero-time distribution is centered in the region of the metastable LE-like minimum, and the evolution (solvent relaxation) drives the system towards the thermodynamically stable minimum having CT character. Having no barrier to cross, the dynamics is completely governed by the solvation time.

Based on transient distributions, differential absorption spectra can be obtained as the difference in the UV-vis absorbance (as measured by the probe beam) of the optically pumped system and the system at rest. The absorbance

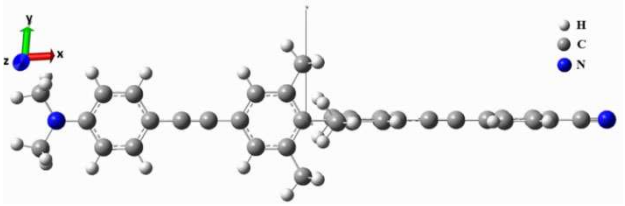

Figure 9. Optimized structure of TBP in gas phase.

variation (ΔA) has positive contributions from ESA and negative contributions from ground-state bleaching and stimulated emission.

In our three-state model, excited-state absorption cannot be evaluated, due to the lack of excited states beyond the two explicitly accounted for. In order to be able to calculate the excited-state absorption contribution, we thus introduce two ad-hoc higher-energy excited states: one, having a transition dipole moment from the LE state and not being solvatochromic, such as the LE state; the other, having a transition dipole moment from the CT state and having the same solvatochromic behavior as the CT state itself. The calculated transient absorption spectra (including also the contributions from bleaching and stimulated emission) are reported in Figure 8. The agreement with the experimental behavior is impressive, demonstrating that solvation governs the dynamics of the transient spectra, being faster in diethyl ether, slightly slower in DMSO and very much slower in triacetin, according to the respective solvation times (1.7 ps for diethyl ether,[51] 3.1 ps for DMSO,[52] 80 ps for triacetin[53]). In particular, solvation drives the population from the initially populated LE state to the CT state; from the LE state, excited-state absorption leads to a state having LE character (non-solvatochromic), while, from the CT state, excited-state absorption leads to a state having the very same solvatochromic behavior (i.e. another state having CT character). The solvation-driven evolution of the population from the LE to the CT state induces an intensity exchange between the two excited-state absorption bands, which cross in an isosbestic point, proving that transitions between excited states having different nature is not allowed.

To support our interpretation, we performed quantum chemical calculations, retrieving the energies of a large number of excited states in order to study their nature.

2.5. Quantum-Chemical Computations

To model the TBP molecule for theoretical calculations, we have substituted the long chain alkyl groups in the amino moiety with methyl groups, in the assumption that this has marginal spectroscopic effects. The optimized structure of the molecule in gas phase is reported in Figure 9, showing that the biphenyl moiety is twisted along the central C–C bond by ~90°, in agreement with the crystallographic structure of other substituted-biphenyl molecules.[27] This twist hinders the conjugation of the π cloud across the twisted bridge. The ground state

Table 3. TDDFT Results for TBP in Gas phase and different solvents.

	Transition	Wavelength [nm]/energy [eV]	Oscillator Strength	Nature of Transitions (MO Contributions)
gas phase	S0→S1	308/4.02 (LE)	3.03	H-1→L (38%) H→L+1 (52%)
	S0→S2	293/4.23	0.01	H-1→L (53%) H→L+1 (37%)
	S0→S3	273/4.53 (CT)	0.00	H→L (87%)
cHex	S0→S1	315/3.93 (LE)	3.26	H-1→L (35%) H→L+1 (55%)
	S0→S2	302/4.10	0.03	H-1→L (56%) H→L+1 (35%)
	S0→S3	274/4.52 (CT)	0.00	H→L (88%)
toluene	S0→S1	316/3.92 (LE)	3.28	H-1→L (35%) H→L+1 (56%)
	S0→S2	303/4.09	0.04	H-1→L (57%) H→L+1 (34%)
	S0→S3	274/4.52	0.06	H→L+7 (70%)
	S0→S4	274/4.52 (CT)	0.00	H→L (88%)
DCM	S0→S1	322/3.34 (LE)	3.24	H-1→L (25%) H→L+1 (65%)
	S0→S2	312/3.97	0.17	H→L+6 (66%) H→L+1 (25%)
	S0→S3	278/4.46	0.09	H→L+6 (67%)
	S0→S4	273/4.55 (CT)	0.00	H→L (89%)

geometry was also optimized in different solvents (cyclohexane, toluene and dichloromethane) obtaining similar results.

To look into the transition energies of TBP in different solvents and in gas phase, we carried out TD-DFT calculations: Table 3 summarizes the first few low-energy transitions. Several flavors of PCM models are available and we adopted the state-specific approach,[57] which takes into account the variations of the polarization of the solvent following the electronic density rearrangements of the solute.[58]

Results in Table 3 are consistent with experimental results, showing a non-solvatochromic absorption. Irrespective of the polarity of the solvent, the first transition (S0→S1) is a LE transition with an almost equal weight of two localized excitations on the donor fragment (H→L+1) and on the acceptor fragment (H-1→L), see Figures 10 and S1, blue arrows.

The first CT state is found at higher energy, corresponding to S3 in gas phase and in cyclohexane and to S4 in toluene and DCM. This CT state corresponds to the H→L transition, displacing charge from the D to the A site (Figures 10 and 11, red arrows). The vertical energy of the CT state is marginally affected by the solvent polarity, as expected (indeed the negligible polarity of the molecule in the ground state implies a negligible value of the corresponding equilibrium reaction field). For such a large molecule, geometry optimization in the excited state is computationally very expensive and we just succeeded to optimize the geometry in the gas phase, but we could not calculate vibrational frequencies. Accordingly, we cannot confirm that the CT state becomes the fluorescent states in polar solvents. However, the permanent dipole moment calculated for the vertical lowest CT state is very large (61 and 72 D in gas phase and DCM, respectively, against a ground-state dipole moment <10 D). This highly polar excited state is expected to be strongly stabilized in polar solvents due to solvent relaxation. While we cannot obtain the relaxed excited

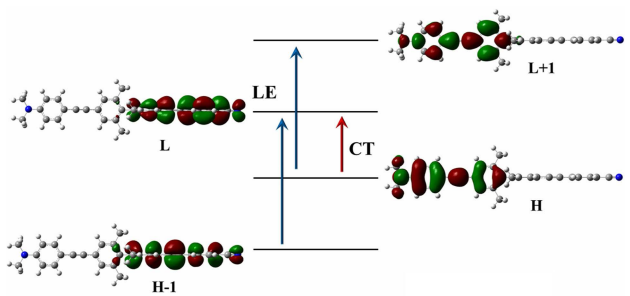

Figure 10. Frontier Molecular Orbitals of TBP in gas phase (TDDFT level) and the LE/CT transitions. Blue arrow indicates LE transition and red arrow indicates CT transition.

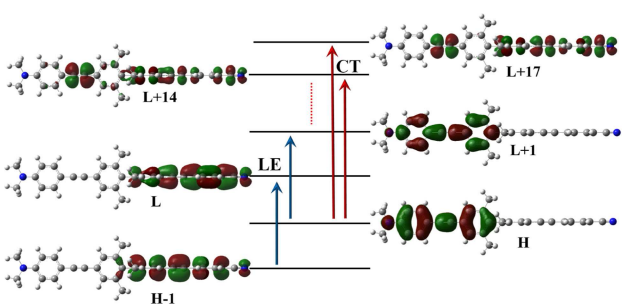

Figure 11. Frontier Molecular Orbitals of TBP obtained with ZINDO calculations showing the LE/CT transitions. Blue arrow indicates LE transition and red arrow indicates CT transition.

state, a solvent relaxation energy of ~0.5 eV, corresponding to a mildly polar solvent, is enough to stabilize the CT state below the lowest-energy LE state, as also confirmed by the essential-state modeling.

To discuss ESA spectra we must address higher-energy excited states, implying a very expensive calculation within TD-DFT, which could not be undertaken. We therefore made resort to semiempirical ZINDO/S calculations in gas phase, as implemented in the Gaussian09 package.[59] In this way, we were able to reach states with energies up to 7 eV (180 nm) above the ground state, comparable to the energy of the excited states addressed in transient spectroscopy (neither the computational results nor the experimental ones suggest any ionization effect at these energies). Computational results for highly excited states should be taken with care, and they cannot be directly compared with experiment. Indeed, we just exploit them to validate and generalize the hypothesis, suggested by experimental data, of the existence of two sets of optically independent excited states.

In Table 4, we show ZINDO/S results for a few low-lying transitions of TBP in gas phase. In comparison with experimental data, the energy of the first allowed transition is underestimated in gas phase by ~0.3 eV. The lowest-energy LE and CT states (as labelled in Table 4) have been identified by analyzing the nature of the MOs most contributing to each transition (see Figure 11). ZINDO results are in line with TD-DFT results, ascribing a LE character to the lowest-energy transition (S0→S1, calculated at 3.47 eV, i.e. 357 nm). The first transition with CT character is calculated in ZINDO/S at 4.34 eV (285 nm) as the S0→S9 transition. Having identified the first LE and CT states as S1 and S9, respectively, we calculated the transition dipole moments (and more precisely their Cartesian components μ_{ti}, $i=x,y,z$, see Supporting Information, Table S1 and S2) from those two states towards higher-energy states. We verified that the only significant component of μ_t is the one aligned along the molecular axis (assigned to the x direction). In Table 5, we have tabulated the transition energies from the first LE state (S1) and from the first CT state (S9) to higher states, selecting the ones with sizeable μ_{tx} values. The MO's taking part in these transitions have also been checked to verify the nature of each transition.

Table 4. ZINDO Results for TBP showing the first few low energy transitions.

Transition	Wavelength [nm]/ energy [eV]	Oscillator strength	Nature of transitions (MO contributions)
S0→S1	357/3.47 (LE)	1.91	H-1→L (33%) H→L+1 (43%)
S0→S2	352/3.53	0.00	H-8→L (56%)
S0→S3	344/3.60	0.00	H-5→L+1 (59%)
S0→S4	342/3.62	0.01	H-1→L (39%) H→L+1 (33%)
S0→S5	307/4.04	0.05	H→L+6 (69%)
S0→S6	302/4.11	0.01	H→L+5 (37%)
S0→S7	299/4.14	0.00	H-1→L+4 (45%)
S0→S8	291/4.26	0.00	H-9→L (34%) H-1→L+2 (41%)
S0→S9	285/4.34 (CT)	0.00	H→L+14 (37%) H→L+17 (23%)
S0→S10	280/4.43	0.00	H→L+11 (57%)

Table 5. Transition dipole moments and energies from the lowest-energy LE state (S1) to higher-energy LE states and from the lowest-energy CT state (S9) to higher-energy CT states.

Lowest LE state	Higher LE states	μ_{tx} [a.u.]	ΔE [eV]/λ [nm]
S1	S4	0.3062	0.27/4592
	S12	1.0317	1.23/1008
	S14	0.8502	
	S22	−3.0683	
	S24	1.8033	1.99/623
	S26	3.0691	
	S32	−0.9658	2.30/539
	S33	−0.6430	
	S40	0.8957	2.64/470
	S41	−0.6838	
	S57	0.3845	3.02/410
	S60	−0.3162	
	S66	0.2124	
	S69	0.3696	
Lowest CT State	**Higher CT States**	**μ_{tx} [a.u.]**	**ΔE/λ [eV/nm]**
S9	S13	−1.1938	0.39/3180
	S30	0.2932	1.30/954
	S31	−0.5346	
	S37	0.7922	1.54/805
	S52	−0.3681	1.97/630
	S53	0.2252	
	S55	−0.3640	
	S67	0.7169	2.33/532
	S71	0.1052	

Data in Table 5 demonstrate that the excited states that can be reached from S1 (the lowest-energy LE state) are different from those that can be reached from S9 (the lowest-energy CT state). In particular, the states reachable upon photoexcitation from S1 have a predominant LE nature and those reachable upon photoexcitation from S9 have a predominant CT nature. This result confirms and generalizes the optical independence of CT and LE states suggested by transient spectroscopy.

3. Conclusions

We have presented a thorough spectroscopic characterization of a biphenyl-based push-pull chromophore, by means of UV-vis absorption and emission spectroscopy, as well as pump-probe transient spectroscopy. The substitution of the 2,2′ and 6,6′ positions of the biphenyl moiety imposes the orthogonality of the two phenyl rings, decoupling the electron transfer from the donor to the acceptor site from torsional/vibrational degrees of freedom. In this way, solvation remains as the only relevant degree of freedom coupled to the charge transfer. Experimental data, supported by theoretical modeling through an essential-state description, suggest a subtle interplay between a LE state and a CT state. The CT state is sensitive to solvent polarity and is characterized by a fairly long lifetime (~10 ns). Polar solvation governs the relative energy of the two relaxed excited states, and therefore the dynamics following photoexcitation.

Interestingly, transient absorption data suggest that transitions are allowed only between states having the same (LE or CT) nature. This interpretation is supported by quantum chemical calculations addressing excited states up to very high energies: two different manifolds of states can be recognized, having LE or CT nature, not interconverted via optical excitation. However, a spontaneous evolution from the lowest-energy LE state to the lowest-energy CT state is allowed in polar solvents and is driven by the solvent relaxation.

While other donor-acceptor systems are known to behave in a similar way, with a LE/CT interplay revealed by dual fluorescence and by transient-absorption data, here we investigated for the first time an elongated donor-acceptor molecule where π-conjugated bridges act as linkers and assure long-distance electron transfer. The long-distance charge-separated state, moreover, is surprisingly long-lived (both in polar solvents and in the solid state), most probably as a result of the blocked conformation of the central biphenyl core, which is substituted by sterically hindering methyl groups.

To the best of our knowledge, here we offer for the first time a convincing demonstration of the presence of two sets of optically-independent excited states, having either LE or CT character. The two sets can only "communicate" thanks to solvation, which is the only driving force for the charge-separation process.

Experimental Section

Synthesis

1,2-Bis(3,5-dimethylphenyl)hydrazine (**2**): Zinc powder (25.04 g, 0.393 mol) was added to a suspension of 3,5-dimethylnitrobenzene (**1**) (10.01 g, 66.2 mmol) in EtOH (40 mL) under argon. The mixture was refluxed until a solution was obtained. Heating was removed and a solution of NaOH (15.06 g, 0.376 mol) in water (50 mL) was added dropwise, in order to maintain the reflux. After addition of about one third of NaOH, heating was needed again, and after addition was complete, the mixture was refluxed for 2 h. Zinc powder was then added again (10.08 g, 0.153 mol), and the mixture was refluxed for another 2 h. The hot suspension was filtered through Celite and washed with hot EtOH (60 mL) into a mixture of AcOH (45 mL), water (105 mL) and sodium bisulfite (1.0 g). The solution was cooled with a cold water bath, and the precipitate was filtered off and recrystallized from heptane to give 3.501 g (44%) of **2**.[36,37] ^{1}H NMR (300 MHz, $CDCl_3$): $\delta = 6.51$ (s, 6 H), 5.48 (br s, 2 H), 2.26 (s, 12H).

2,2′,6,6′-Tetramethylbenzidine (**3**): A solution of 1,2-bis(3,5-dimethylphenyl)hydrazine (**2**) (3.502 g, 14.57 mmol) in 165 mL of HCl (10%) was bubbled with argon for 20 min, and refluxed for 2 h. The mixture was cooled to rt, and a solution of NaOH (30 g in 120 mL of water) was added dropwise until pH ~10–11. The product was extracted with ether (3x). The combined organic layers were washed with brine until neutral pH, dried with Na_2SO_4, filtered and evaporated under reduced pressure. The crude product was purified by column chromatography on silica gel (EtOAc/heptane 1:2), to give 2.316 g (66%) of **3**.[36,37] ^{1}H NMR (300 MHz, $CDCl_3$): $\delta =$ 6.49 (s, 4 H), 3.53 (br s, 4 H), 1.83 (s, 12 H).

4,4′-Diiodo-2,2′,6,6′-tetramethylbiphenyl (**4**): A solution of $NaNO_2$ (0.875 g, 12.68 mmol) in water (3 mL) was added to a suspension of 1,2-bis(3,5-dimethylphenyl)hydrazine (**3**) (1.386 g, 5.767 mmol) in water (22 mL) and sulfuric acid (97%, 12 mL) cooled in an ice bath. The mixture was stirred at ~5 °C for 30 min, and a solution of I_2 (4.142 g, 16.32 mmol) and KI (4.579 g, 27.58 mmol) in water (7.5 mL) was added. The mixture was stirred for another 20 min at ~5 °C. Water (30 mL) and CH_2Cl_2 (75 mL) were added, and the solution was stirred at rt overnight. Sodium thiosulfate (4.89 g) was added, and the mixture was stirred for 10 min. The precipitate was filtered off and washed with CH_2Cl_2. The two layers were separated and the aqueous layer was extracted with CH_2Cl_2 (2×45 mL). The combined organic layers were then washed again (3x) with sodium thiosulfate and brine, and finally dried with $MgSO_4$. The solvent was removed under reduced pressure, and the crude product was purified by column chromatography on silica gel (heptane), to give 1.805 g (68%) of **4**.[37,38] ^{1}H NMR (300 MHz, $CDCl_3$): $\delta = 7.49$ (s, 4 H), 1.84 (s, 12 H).

4-[(4′-Iodo-2,2′,6,6′-tetramethyl[1,1′-biphenyl]-4-yl)ethynyl]-N,N-dihexyl-benzenamine (**6**): A solution of 4,4′-diiodo-2,2′,6,6′-tetramethylbiphenyl (**4**) (0.8074 g, 1.749 mmol) and *N*,*N*-dihexyl-4-[2-(trimethylsilyl)ethynyl]-benzenamine[39] (**5**) (0.1795 g, 0.503 mmol) in toluene (5 mL) and Et_3N (1.5 ml) was bubbled with argon for 20 min. CuI (4.8 mg, 0.0175 mmol), $Pd(PPh_3)_2Cl_2$ (13.7 mg, 0.0175 mmol) and TBAF (1 M in THF, 1 mL) were successively added, and the mixture was stirred at 40 °C overnight. Solvents were evaporated and the residue was purified by column chromatography on silica gel, eluting with CH_2Cl_2/heptane (gradient from 5:95 to 20:80), to give 0.1976 g (64%) of **6**. ^{1}H NMR (300 MHz, $CDCl_3$): $\delta = 7.50$ (s, 2H), 7.37 (d, 2H, J = 8.9 Hz), 6.58 (d, 2H, J = 8.9 Hz), 7.29 (s, 2H), 3.28 (t, 4 H, J = 7.6 Hz), 1.88 (s, 6H), 1.86 (s, 6H), 1.53 (m, 4 H), 1.33 (m, 12 H), 0.91 (t, 6H, J = 6.8 Hz); ^{13}C NMR (75 MHz, $CDCl_3$): $\delta = 147.8$, 139.2, 138.4, 138.0, 136.3, 135.4, 132.8, 130.4, 122.9, 111.2, 108.8, 92.6, 90.4, 87.0, 51.0, 31.7, 27.2, 26.8, 22.7, 19.6, 19.3, 14.0; HRMS (ESI, CH_2Cl_2/CH_3OH 90:10): *m/z* calcd for $C_{36}H_{46}NI$: 619.2675 ($M^{+\cdot}$); found: 619.2671.

4-[[4′-[[4-(Dihexylamino)phenyl]ethynyl]-2,2′,6,6′-tetramethyl[1,1′-biphenyl]-4-yl]ethynyl]benzonitrile (**TBP**): A solution of iodo compound **6** (87.3 mg, 0.141 mmol) and 4-[2-(trimethylsilyl)ethynyl] benzonitrile (**7**)[40] (35.3 mg, 0.177 mmol) in toluene (2 mL) and Et_3N (0.5 mL) was bubbled with argon for 20 min. CuI (2 mg, 0.01 mmol), $Pd(PPh_3)_2Cl_2$ (7.4 mg, 0.01 mmol) and TBAF (1 M in THF, 0.5 mL) were successively added, and the mixture was stirred at 40 °C overnight. Solvents were evaporated and the residue was purified by column chromatography on silica gel, eluting with CH_2Cl_2/heptane (1:4), to give 0.0627 g (72%) of **TBP**. ^{1}H NMR (300 MHz, $CDCl_3$): $\delta = 7.66$ (d, 2H, J = 8.7 Hz), 7.61 (d, 2H, J = 8.7 Hz), 7.38 (d, 2H, J = 9.0 Hz), 7.36 (s, 2H), 7.32 (s, 2H), 6.59 (d, 2H, J = 9.0 Hz), 3.29 (t, 4 H, J = 7.7 Hz), 1.93 (s, 6H), 1.90 (s, 6H), 1.60 (m, 4 H), 1.34 (m, 12 H), 0.92 (t, 6H, J = 6.7 Hz); ^{13}C NMR (75 MHz, $CDCl_3$): $\delta = 148.0$, 141.3, 138.7, 136.3, 135.5, 133.0, 132.2, 132.1, 131.0, 130.6, 128.6, 123.1, 120.7, 118.7, 111.3, 108.9, 94.4, 90.6, 87.4, 87.1, 51.1, 31.9, 27.3, 27.0, 22.8, 19.8, 19.7, 14.2; HRMS (ESI, CH_2Cl_2/CH_3OH 90:10): *m/z* calcd for $C_{45}H_{51}N_2$: 619.4052 ($[M+H]^+$); found: 619.4047.

Preparation of Organic Nanoparticle Suspensions

200 μL of a 1 mM THF solution of the compound was added to 9.800 mL of bidistilled water under vigorous stirring, to achieve a final nominal concentration of 2×10^{-5} M. The suspension was kept under vigorous stirring for about 15 minutes.

Absorption and Fluorescence Spectroscopy

Absorption and emission measurements were performed at room temperature on freshly prepared solutions. For fluorescence

measurements, the optical density was kept ≤ 0.1 (roughly corresponding to a 10^{-6} M) concentration, in order to minimize inner-filter effects. All solvents were spectroscopic or HPLC grade and were used as received. Absorption measurements were performed with a Perkin-Elmer Lambda 650 double-beam UV/Vis spectrophotometer. To estimate the molar extinction coefficients in chloroform, the Lambert-Beer law was verified in the concentration range 10^{-4}–10^{-6} M. Fully corrected steady-state emission and excitation spectra were obtained with a Fluoromax-3 Horiba Jobin-Yvon fluorometer (detection at 90 degrees) equipped with a Xenon lamp as the excitation source. A diluted solution ($c \sim 10^{-6}$ M) of fluorescein in NaOH(aq) 0.1 M ($\phi = 0.9$, $\lambda_{exc} = 460$ nm) was used as reference standard for the determination of the fluorescence quantum yields. In order to integrate the emission spectra for evaluating the quantum yield, even in the cases where the spectra were not "complete" because we had to stop measuring at 670 nm, the spectra were fitted (on the wavenumber scale) with Gaussian lines. The emission spectrum of the powders was collected placing the sample on a front-face vertical sample holder, with an inclination of the plane of 30 degrees with respect to the propagation direction of the incoming light; an excitation and an emission polarisers were placed at the magic angle, in order to decrease the scattered light on the detector. Fluorescence decays were measured with the TCSPC (Time-Correlated Single-Photon Counting) technique, using the Fluoromax-3 instrument equipped with a Horiba Fluoro-Hub analyzer. A pulsed NanoLed at $\lambda =$ 340 nm was used as the excitation source. The prompt signal was acquired by measuring the scattering of an aqueous suspension obtained by adding two drops of Ludox HS-40 (Sigma-Aldrich) to approximately 4 mL of water. Lifetimes (τ) values were extracted by reconvolution analysis of the decay profiles and the goodness of the fit was evaluated with the chi-square test (results were retained if $\chi^2 < 1.2$).

Transient Absorption Spectroscopy

The apparatus used for the transient absorption spectroscopy measurements is based on a Ti:sapphire regenerative amplifier (BMI Alpha 1000) system pumped by a Ti:sapphire oscillator (Spectra Physics Tsunami). The system produces 100 fs pulses at 785 nm, 1 kHz repetition rate and average power of 450 mW. Excitation pulses at 330 nm have been obtained by pumping an optical parametric amplifier (TOPAS, light conversion) by a portion of the fundamental 785 nm. The output of the TOPAS has been first frequency doubled and then mixed with residual 800 nm radiation to generate the desired pump wavelength. The probe pulse was generated by focusing a small portion of the fundamental laser output radiation on a 2 mm thick sapphire window. The pump beam polarization has been set to magic angle with respect to the probe beam by rotating a $\lambda/2$ plate. Excitation powers were on the order of 100 nJ. Pump-probe delays were introduced by sending the probe beam through a motorized stage. Multichannel detection was achieved by sending the white light continuum after passing through the sample to a flat field monochromator coupled to a home-made CCD detector. Measurements were carried out in a 2 mm thick quartz cell. To avoid sample photodegradation and multiple photon excitation, the solution was refreshed using magnetic stirring. Data were analysed through singular value decomposition and global analysis performed using the software Glotaran.[60]

Computational Details

All the quantum chemical calculations for TBP in gas phase and solvents have been carried out using Density Functional Theory (DFT) and Time Dependent DFT (TDDFT) as implemented in the Gaussian 09 package.[59] The 6-31+g(d) basis set was adopted for all calculations and a long-range Coulomb attenuated functional CAM-B3LYP[61] was used both for geometry optimization and for the calculation of vertical excited states. Calculation were run in gas phase and in dichloromethane (DCM), cyclohexane and toluene, in the polarizable continuum model (PCM)[62] approach (non-equilibrium, state-specific) as implemented in Gaussian 09 package. The optimized ground state (S0) geometries have been confirmed to be in local minimum energy structures by analyzing the vibrational frequencies in the ground state. To look into the excited state geometry in gas phase for TBP, optimization of the first charge transfer (CT) state and the first local excited state (LE) were carried out using the above-mentioned level of theory. We tried to look into the optimized geometry of the excited state even in solvent, but due to computational limitations and heavy nature of the calculations, it could not be achieved. Since we are interested to the calculation of high-energy excited states, a task that becomes too expensive in TDDFT, we have resorted to the semi-empirical ZINDO calculations, as implemented in G09, to look into the nature of the transitions.

Acknowledgements

The authors gratefully acknowledge financial support from the Italian Ministero dell'Istruzione, dell'Università e della Ricerca (MIUR): grant RBFR10Y5VW (FIRB Futuro in Ricerca 2010) and grant "Dipartimenti di Eccellenza" (DM 11/05/2017 n. 262). This project has received funding from the European Union's Horizon 2020 research and innovation programme under grant agreement No 812872 (TADFlife). This research benefits from the HPC (High Performance Computing) facility of the University of Parma, Italy. We thank Cédric Rouxel and Cynthia Vandermeulen for assistance in the synthesis of TBP.

Conflict of Interest

The authors declare no conflict of interest.

Keywords: electron transfer · dual fluorescence · solvation dynamics · time-resolved spectroscopy · theoretical modelling

[1] M. Mamedov, Govindjee, V. Nadtochenko, A. Semenov, *Photosynth. Res.* **2015**, *125*, 51–63.
[2] H. Klauk, *Organic Electronics: Materials, Manufacturing and Applications*, Wiley-VCH, **2006**.
[3] L. Venkataraman, J. E. Klare, C. Nuckolls, M. S. Hybertsen, M. L. Steigerwald, *Nature* **2006**, *442*, 904–907.
[4] A. P. Kulkarni, C. J. Tonzola, A. Babel, S. A. Jenekhe, *Chem. Mater.* **2004**, *16*, 4556–4573.
[5] S. Günes, H. Neugebauer, N. S. Sariciftci, *Chem. Rev.* **2007**, *107*, 1324–1338.
[6] B. Kippelen, J.-L. Brédas, *Energy Environ. Sci.* **2009**, *2*, 251.
[7] V. May, O. Kühn, *Charge and Energy Transfer Dynamics in Molecular Systems*, Wiley-VCH, **2011**.
[8] T. Kumpulainen, B. Lang, A. Rosspeintner, E. Vauthey, *Chem. Rev.* **2017**, *117*, 10826–10939.
[9] C. A. Rumble, M. Maroncelli, *J. Chem. Phys.* **2018**, *148*, 193801.
[10] K. A. Zachariasse, S. I. Druzhinin, O. Morawski, B. Kozankiewicz, *J. Phys. Chem. A* **2018**, *122*, 6985–6996.

[11] K. K. Mentel, A. Serra, P. E. Abreu, L. G. Arnaut, *Nat. Commun.* **2018**, *9*, 2903.
[12] W. Schuddeboom, S. A. Jonker, J. M. Warman, U. Leinhos, W. Kuehnle, K. A. Zachariasse, *J. Phys. Chem.* **1992**, *96*, 10809–10819.
[13] K. A. Zachariasse, M. Grobys, T. von der Haar, A. Hebecker, Y. V. Il'ichev, Y.-B. Jiang, O. Morawski, W. Kühnle, *J. Photochem. Photobiol. A* **1996**, *102*, 59–70.
[14] K. A. Zachariasse, S. I. Druzhinin, W. Bosch, R. Machinek, *J. Am. Chem. Soc.* **2004**, *126*, 1705–1715.
[15] S. Murali, V. Kharlanov, W. Rettig, A. I. Tolmachev, A. V. Kropachev, *J. Phys. Chem. A* **2005**, *109*, 6420–6429.
[16] N. Nakashima, M. Murakawa, N. Mataga, *Bull. Chem. Soc. Jpn.* **1976**, *49*, 854–858.
[17] S. A. Kovalenko, J. L. Pérez Lustres, N. P. Ernsting, W. Rettig, *J. Phys. Chem. A* **2003**, *107*, 10228–10232.
[18] M. Jurczok, P. Plaza, M. M. Martin, Y. H. Meyer, W. Rettig, *Chem. Phys.* **2000**, *253*, 339–349.
[19] M. Jurczok, P. Plaza, W. Rettig, M. M. Martin, *Chem. Phys.* **2000**, *256*, 137–148.
[20] N. Mataga, H. Yao, T. Okada, W. Rettig, *J. Phys. Chem.* **1989**, *93*, 3383–3386.
[21] S. Hashimoto, A. Yabushita, T. Kobayashi, K. Okamura, I. Iwakura, *Chem. Phys.* **2018**, *512*, 128–134.
[22] W. Rettig, M. Maus, R. Lapouyade, *Berichte der Bunsengesellschaft für Phys. Chemie* **1996**, *100*, 2091–2096.
[23] M. Maus, W. Rettig, G. Jonusauskas, R. Lapouyade, C. Rullière, *J. Phys. Chem. A* **1998**, *102*, 7393–7405.
[24] M. Maus, W. Rettig, D. Bonafoux, R. Lapouyade, *J. Phys. Chem. A* **1999**, *103*, 3388–3401.
[25] M. Maus, W. Rettig, *J. Phys. Chem. A* **2002**, *106*, 2104–2111.
[26] J. Dobkowski, M. Kijak, I. V. Sazanovich, J. Waluk, *J. Phys. Chem. B* **2015**, *119*, 7294–7307.
[27] D. Vonlanthen, J. Rotzler, M. Neuburger, M. Mayor, *Eur. J. Org. Chem.* **2010**, *2010*, 120–133.
[28] W. Weigel, W. Rettig, M. Dekhtyar, C. Modrakowski, M. Beinhoff, A. D. Schlüter, *J. Phys. Chem. A* **2003**, *107*, 5941–5947.
[29] S. Sasaki, G. P. C. Drummen, G. Konishi, *J. Mater. Chem. C* **2016**, *4*, 2731–2743.
[30] O. Mongin, L. Porrès, M. Charlot, C. Katan, M. Blanchard-Desce, *Chem. Eur. J.* **2007**, *13*, 1481–1498.
[31] F. Bureš, *RSC Adv.* **2014**, *4*, 58826–58851.
[32] L. Donato, A. Mourot, C. M. Davenport, C. Herbivo, D. Warther, J. Léonard, F. Bolze, J.-F. Nicoud, R. H. Kramer, M. Goeldner, *Angew. Chem. Int. Ed.* **2012**, *51*, 1840–1843; *Angew. Chem.* **2012**, *124*, 1876–1879.
[33] J. Cody, C. J. Fahrni, *Tetrahedron* **2004**, *60*, 11099–11107.
[34] M. Gantenbein, M. Hellstern, L. Le Pleux, M. Neuburger, M. Mayor, *Chem. Mater.* **2015**, *27*, 1772–1779.
[35] O. V. Mikhnenko, R. Ruiter, P. W. M. Blom, M. A. Loi, *Phys. Rev. Lett.* **2012**, *108*, 137401.
[36] A. Helms, D. Heiler, G. McLendon, *J. Am. Chem. Soc.* **1992**, *114*, 6227–6238.
[37] D. Vonlanthen, J. Rotzler, M. Neuburger, M. Mayor, *Eur. J. Org. Chem.* **2010**, *2010*, 120–133.
[38] S. Suzuki, R. Sugimura, M. Kozaki, K. Keyaki, K. Nozaki, N. Ikeda, K. Akiyama, K. Okada, *J. Am. Chem. Soc.* **2009**, *131*, 10374–10375.
[39] C. Rouxel, M. Charlot, O. Mongin, T. R. Krishna, A.-M. Caminade, J.-P. Majoral, M. Blanchard-Desce, *Chem. Eur. J.* **2012**, *18*, 16450–16462.
[40] S. P. McIlroy, E. Cló, L. Nikolajsen, P. K. Frederiksen, C. B. Nielsen, K. V. Mikkelsen, K. V. Gothelf, P. R. Ogilby, *J. Org. Chem.* **2005**, *70*, 1134–1146.
[41] J. Saltiel, V. K. R. Kumar, *J. Phys. Chem. A* **2012**, *116*, 10548–10558.
[42] M. Krämer, U. H. F. Bunz, A. Dreuw, *J. Phys. Chem. A* **2017**, *121*, 946–953.
[43] M. Flock, L. Bosse, D. Kaiser, B. Engels, I. Fischer, *Phys. Chem. Chem. Phys.* **2019**, *21*, 13157–13164.
[44] P. Meystre, M. Sargent, in *Elem. Quantum Opt.*, Springer Berlin Heidelberg, Berlin, Heidelberg, **2007**, pp. 51–91.
[45] C. Sissa, V. Calabrese, M. Cavazzini, L. Grisanti, F. Terenziani, S. Quici, A. Painelli, *Chem. Eur. J.* **2013**, *19*, 924–935.
[46] B. Boldrini, E. Cavalli, A. Painelli, F. Terenziani, *J. Phys. Chem. A* **2002**, *106*, 6286–6294.
[47] F. Terenziani, A. Painelli, *Phys. Chem. Chem. Phys.* **2015**, *17*, 13074–13081.
[48] E. R. Henry, *Biophys. J.* **1997**, *72*, 652–673.
[49] E. R. Henry, J. Hofrichter, **1992**, pp. 129–192.
[50] I. H. M. van Stokkum, D. S. Larsen, R. van Grondelle, *Biochim. Biophys. Acta Bioenerg.* **2004**, *1657*, 82–104.
[51] E. R. Middelhoek, H. Zhang, J. W. Verhoeven, M. Glasbeek, *Chem. Phys.* **1996**, *211*, 489–497.
[52] M. A. Kahlow, T. J. Kang, P. F. Barbara, *J. Phys. Chem.* **1987**, *91*, 6452–6455.
[53] G. C. Walker, E. Aakesson, A. E. Johnson, N. E. Levinger, P. F. Barbara, *J. Phys. Chem.* **1992**, *96*, 3728–3736.
[54] F. Terenziani, A. Painelli, *Chem. Phys.* **2003**, *295*, 35–46.
[55] R. S. Fee, M. Maroncelli, *Chem. Phys.* **1994**, *183*, 235–247.
[56] S. Mukamel, *Principles of Nonlinear Optical Spectroscopy*, Oxford University Press, New York, **1995**.
[57] R. Improta, V. Barone, F. Santoro, *Angew. Chem. Int. Ed.* **2007**, *46*, 405–408; *Angew. Chem.* **2007**, *119*, 409–412.
[58] D. Jacquemin, A. Planchat, C. Adamo, B. Mennucci, *J. Chem. Theory Comput.* **2012**, *8*, 2359–2372.
[59] M. J. Frisch, G. W. Trucks, H. B. Schlegel, G. E. Scuseria, M. A. Robb, J. R. Cheeseman, G. Scalmani, V. Barone, B. Mennucci, G. A. Petersson, *Gaussian 09, Revis. D.01, Gaussian, Inc., Wallingford CT* **2009**.
[60] J. J. Snellenburg, S. P. Laptenok, R. Seger, K. M. Mullen, I. H. M. van Stokkum, *J. Stat. Softw.* **2012**, *49*, DOI 10.18637/jss.v049.i03.
[61] T. Yanai, D. P. Tew, N. C. Handy, *Chem. Phys. Lett.* **2004**, *393*, 51–57.
[62] J. Tomasi, B. Mennucci, R. Cammi, *Chem. Rev.* **2005**, *105*, 2999–3094.

Manuscript received: July 16, 2019
Revised manuscript received: August 26, 2019
Accepted manuscript online: August 27, 2019
Version of record online: September 11, 2019